Tectonophysics 655 (2015) 124–138

Contents lists available at ScienceDirect

Tectonophysics

journal homepage: www.elsevier.com/locate/tecto

Seismotectonics and crustal stress field in the Kumaon–Garhwal Himalaya

P. Mahesh [a,b], Sandeep Gupta [a,*], Utpal Saikia [a], S.S. Rai [c]

[a] CSIR-National Geophysical Research Institute, Hyderabad 500 007, India
[b] Institute of Seismological Research, Gandhinagar, Gujarat 382009, India
[c] Earth and Climate Science Program, Indian Institute of Science Education & Research, Pune 411008, India

ARTICLE INFO

Article history:
Received 2 July 2013
Received in revised form 15 April 2015
Accepted 1 May 2015
Available online 6 June 2015

Keywords:
Fault plane solution
Stress inversion
Seismicity
Seismotectonics
Kumaon–Garhwal Himalaya
Gangetic plain

ABSTRACT

We present fault plane solutions of 94 well located small-to-moderate sized (1.5 ≤ ML ≤ 5.4) earthquakes, which occurred in the Kumaon–Garhwal Himalaya during 2005–2008, using P-wave polarity and body wave amplitudes. These earthquakes show a mixture of thrust, normal and strike-slip type mechanism, with a majority of thrust type. Most of the thrust earthquakes occur at a depth of 8–22 km in the Main Central Thrust (MCT) zone and the Lower Himalaya. The spatial distribution of these earthquakes suggest that the strain resulting from the ongoing collision of the Indian plate with the Eurasian plate is being consumed by thrust fault movement mainly on the north dipping Munsiari Thrust and south dipping Tons Thrust. The strike-slip earthquakes are mainly observed in the Lower Himalaya as well as around the Munsiari region in the MCT zone. The normal earthquakes are also observed in different parts of the Kumaon–Garhwal Himalaya and the Gangetic plain. Their occurrence is attributed to the local structure(s) as well as the flexure of the Indian plate. Stress tensor inversion of the calculated fault plane solutions indicates that the maximum compressive stress in the Gangetic plain is N–S directed and near vertical; whereas in the Kumaon–Garhwal Himalaya, it is near horizontal and NNE–SSW directed, and correlating with the prevailing stress condition due to northward movement of Indian plate.

1. Introduction

The Himalayan arc is formed by the northward movement of the Indian plate that continues to push the Eurasian plate since ~50 Ma (Basse et al., 1984; Patriat and Achache, 1984). In the process, it has created several fault systems south of the Indus-Tsangpo Suture Zone (ITSZ), marked by distinct litho-tectonic boundaries. These are, from north to south, the Southern Tibetan Detachment System (STDS), Main Central Thrust (MCT), Main Boundary Thrust (MBT) and Main Frontal Thrust (MFT) (Fig. 1) (Patel et al., 2011a; Thakur, 1993; Valdiya, 1980; Yin, 2006). These thrusts in the Himalayan arc are characterized by topographic breaks, which divide the entire Himalaya into four physiographic subdivisions viz., from north to south, Tethyan Himalaya, Higher (or Great) Himalaya, Lower (or Lesser) Himalaya and Sub (or Outer) Himalaya extending southwards to the Himalayan foredeep, also called the Gangetic plains/Ganga basin (Fig. 1). In depth, the last three faults (MFT, MBT, MCT) are believed to emanate from the top of the underthrusted Indian plate beneath the Himalaya, popularly known as plane of detachment or the Main Himalayan Thrust (MHT, Fig. 1, inset A) (Nelson, 1996; Schulte-Pelkum et al., 2005; Zhao et al., 1993). A mid-crustal ramp has been suggested on the MHT (e.g., Berger et al., 2004; DeCelles et al., 2001; Lavé and Avouac, 2001; Lemonnier et al., 1999; Pandey et al., 1995) and its presence has been reported through various structural cross-sections along the Himalayan arc (e.g., Mugnier et al., 2003; Srivastava and Mitra, 1994). Although varying along the Himalayan arc, in its location and dip, the mid-crustal ramp is located approximately beneath the physiographic boundary between the Lower and Higher Himalaya (Wobus et al., 2006). Detailed geology and tectonics of the Himalaya arc have been reviewed by several researchers (e.g., Avouac, 2003; Molnar, 1990; Yin, 2006).

With the underthrusting of the Indian plate beneath the Eurasian plate at a rapid rate of ~20 mm per year (Jade et al., 2014), the collision force builds up pressure continually to generate earthquakes, some times as large as magnitude (M) 8 or more (Fig. 1 inset B). The historical seismicity of the region prior to year 1800 is not well documented. Subsequent instrumental seismic records and maximum intensity data provide evidence for the occurrence of several significant earthquakes (Fig. 1 inset B), namely the 1803 (Kumaon, M ~7.7), the 1833 (Kathmandu, M ~7.7), the 1897 (Shillong, Mw ~8.1), the 1905 (Kangra, Mw ~7.8), the 1934 (Bihar/Nepal, M ~8.3) and the 1950 (Assam, M ~8.7) earthquakes (Ambraseys and Jackson, 2003; Gahalaut, 2008; Rajendran and Rajendran, 2005). These large magnitude earthquakes in the Himalayan arc seem to rupture the seismogenic part of the MHT beneath the Sub and Lower Himalaya and accumulate strain during the

* Corresponding author. Tel.: +91 40 27012466.
E-mail addresses: pmahesh.isr@gmail.com (P. Mahesh), sandeep.ngri@gmail.com (S. Gupta).

http://dx.doi.org/10.1016/j.tecto.2015.05.016
0040-1951/

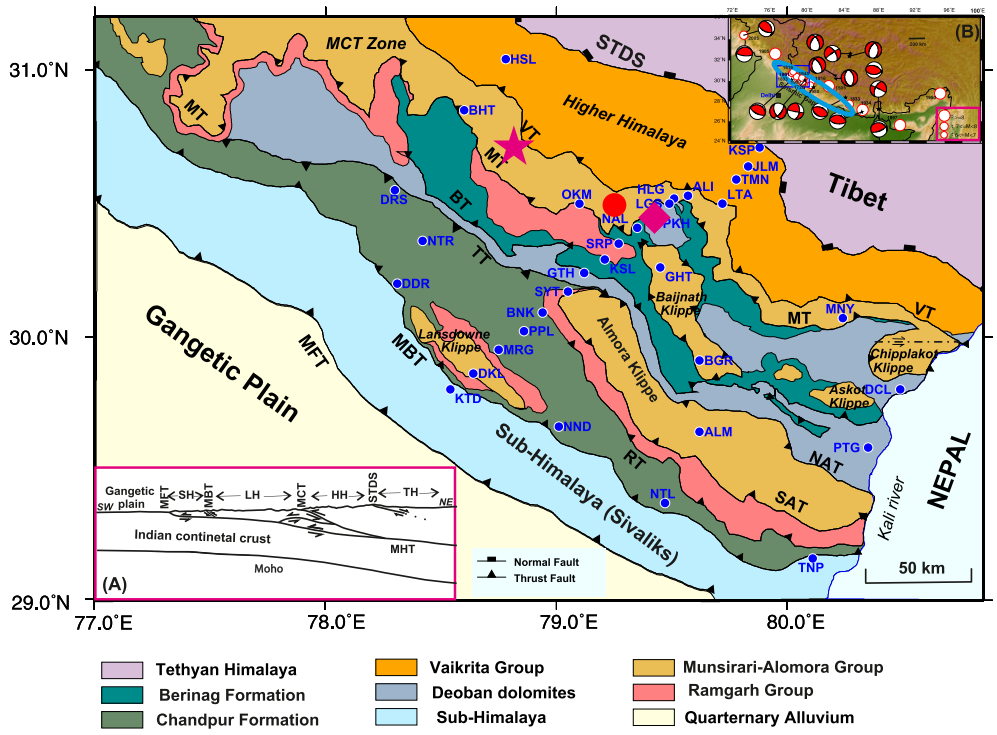

Fig. 1. Geology and tectonic map of study area showing subdivisions of Kumaon–Garhwal Himalaya by major thrusts (continuous lines) viz., MFT: Main Frontal Thrust, MBT: Main Boundary Thrust, MCT: Main Central Thrust, MT: Munsiari Thrust, VT: Vaikrita Thrust, STDS: Southern Tibetan Detachment System, TT: Tons Thrust, RT: Ramgarh Thrust, BT: Berinag Thrust, NAT: North Almora Thrust, SAT: South Almora Thrust. The seismic stations used in the study are shown as filled blue circles. Moderate size earthquakes in the region are shown with different symbols (Star: 1991 Uttarkashi, M 6.6; Diamond: 1999 Chamoli, M 6.3; Circle: 2005 Chamoli, M 5.3). Insert A: A schematic cross section across the Himalaya (modified from Avouac, 2007). SH: Sub Himalaya, LH: Lower Himalaya, HH: Higher Himalaya, TH: Tethyan Himalaya. Insert B: The topography map of Himalaya showing historical earthquakes (circles along with the year of occurrence), central seismic gap (blue ellipse; Seeber and Armbruster, 1981), focal mechanisms of the earthquakes (Harvard CMT Data Base), which occurred during our experiment period (2005–2008); and the present study region (small rectangle).

inter-seismic period, when it is locked. Whereas, small and moderate earthquakes occur on the downdip part of the seismogenic MHT or on the mid-crustal ramp, which connects the gentle dipping seismic and aseismic (lying under the Higher and Tethys Himalaya) parts of the MHT (e.g., Avouac, 2003; Gahalaut, 2008; Molnar, 1990; Seeber and Armbruster, 1981). Recently, lateral variation in the mid-crustal ramp on the MHT in the NW-Himalaya (Patel and Carter, 2009; Singh et al., 2012) and Nepal Himalaya (Robert et al., 2011) have also been reported.

Along the Himalayan arc, there is spatial variation in the seismicity and rupture extents of the large magnitude earthquakes. The locations of rupture areas of the large magnitude earthquakes show seismic gaps along the Himalayan arc. One such seismic gap has been identified between the rupture zones of the 1905 Kangra and the 1934 Bihar great earthquakes (Fig. 1 inset B) and referred as Central Seismic Gap (Bilham et al., 2001; Seeber and Armbruster, 1981). The Kumaon–Garhwal Himalaya (77°–81°E, west of Nepal Himalaya), the focus of present investigation, falls in this ~700 km long seismic gap. This region had experienced significant seismicity (discussed in Section 2.2), and is a part of high earthquake risk zone in the Himalayan arc. The modeling results and geological data suggest that the entire accumulated deformation over interseismic time has not been released (Berger et al., 2004). Geodetic and microseismicity observations indicate the building up of stress and strain in this part of Himalaya capable of generating great earthquake(s) along the MHT (Banerjee and Burgmann, 2002; Bilham et al., 2001; Jade et al., 2014).

To study the seismotectonics and the regional stress pattern in the Kumaon–Garhwal Himalaya, we compute focal mechanism solutions of the well located 94 earthquakes from an earlier study by Mahesh et al. (2013) and use them to understand the regional stress pattern in the region.

2. Overview of Kumaon–Garhwal Himalaya

2.1. Tectonic setting

Following the tectonic framework of the Himalayan arc, the MCT zone in Kumaon–Himalaya is bounded by the Munsiari Thrust (MT) in the south and by the Vaikrita Thrust (VT) in the north (Valdiya, 1980) (Fig. 1). Other major fault systems include the Tons Thrust (TT), Berinag Thrust (BT), Ramgarh Thrust (RT), North Almora Thrust (NAT), and South Almora Thrust (SAT) (Fig. 1). Among these the TT and NAT are the south dipping thrusts, whereas the other thrusts are the north dipping thrusts. Thermochronological studies in the Kumaon–Garhwal Himalaya show spatial and temporal variations in tectonic and exhumation (Patel et al., 2011b; Singh et al., 2012). Recently, the MHT as having flat-ramp-flat geometry is mapped in Kumaon–Garhwal Himalaya using receiver function analysis (Caldwell et al., 2013). This mid-crustal ramp is mapped beneath the MT and dips at an angle of ~16°. Detailed geology and tectonics of the region have been reviewed by several authors (e.g., Célérier et al., 2009; Singh et al., 2012; Srivastava and Mitra, 1994; Valdiya, 1980; Yin, 2006).

2.2. Seismicity and fault plane solutions

The Kumaon–Garhwal Himalaya region, in the Central Himalaya seismic gap, is a part of high earthquake risk zone, where no great earthquake has occurred in the last two centuries. The latest great earthquake possibly occurred in 1803 in Kumaon region and the other possibly in the year 1255 (Bilham et al., 1995). Paleo-seismological studies and historical seismic records indicate possibility of other big earthquake(s) in the past in this region (Ambraseys and Jackson, 2003; Kumar et al.,

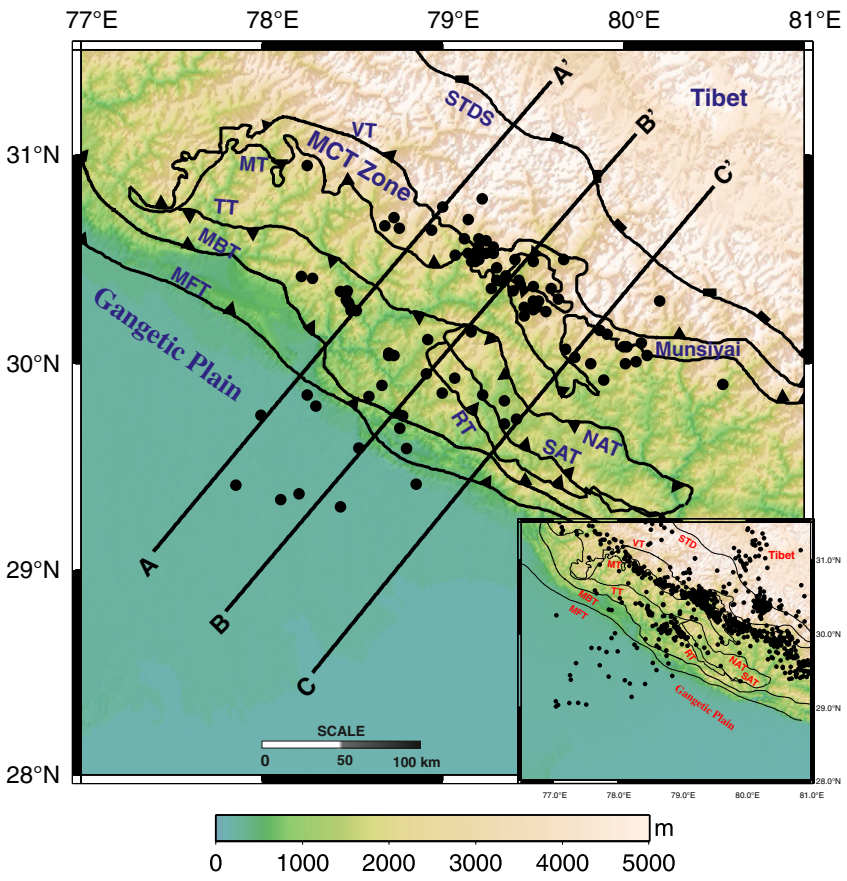

Fig. 2. Epicentral distribution of the 94 earthquakes (filled circles), out of 1150 earthquakes (insert, from Mahesh et al., 2013), used for calculating fault plane solutions. The major tectonic units are same as in Fig. 1. AA′, BB′ and CC′ are three profiles along which focal mechanism solutions are discussed in Fig. 9.

2006). Over the past two decades this region had several moderate to strong ($5.0 < M < 7.0$) earthquakes; the most prominent being the 1991 Uttarkashi (M 6.6), 1999 Chamoli (M 6.3) and 2005 Chamoli (M 5.3) earthquakes (Fig. 1).

Recently, using local earthquakes recorded by a dense network of 50 broadband seismographs in the region during 2005–2008, Mahesh et al. (2013) present a detailed seismicity map for the region (Fig. 2 inset). The salient features of the study are — (i) occurrence of the majority (~75%) of earthquakes in the upper 20 km of the crust, largely above the MHT, (ii) the earthquake epicenter follows an ~10 km wide band along the surface trace of the MT, the southern boundary of the MCT zone, (iii) a parallel band of seismicity along a small segment of the TT, (iv) two seismic clusters — at the STDS and in southern Tibet, and (v) diffused seismic activity in the Gangetic plain.

In this region, unlike other parts of the Himalayan arc, only a few focal mechanism studies have been carried out (e.g., Gaur et al., 1985; Kayal, 1996, 2001; Kayal et al., 2003; Khattri, 1992; Khattri et al., 1989; Paul et al., 2010). These studies are mostly confined to the MCT zone. The focal mechanisms along with seismicity pattern show strong evidence for along the strike heterogeneity, both in terms of spatial segmentation and the source mechanism (Kayal, 2001). Khattri et al. (1989) and Khattri (1992), using micro earthquakes, report two composite fault-plane solutions, one strike-slip faulting and the other thrust faulting in this region. Gaur et al. (1985) report a strike-slip faulting for the microearthquakes for those that occurred at depths less than 10 km in the Garhwal Himalaya. Using aftershock data of the 1991 Uttarkashi (M 6.3) and the 1999 Chamoli (M 6.5) earthquakes in the Garhwal Himalaya; Kayal (1996) and Kayal et al. (2003) report composite fault plane solutions showing both thrust as well strike-slip faulting associated with different active faults. Paul et al. (2010) use five station network data recorded between 1999–2005 near Almora (eastern part of the Kumaon–Garhwal Himalaya) in the Lower Kumaon Himalaya and report composite solutions of the micro earthquakes showing strike-slip faulting for the shallower (depth <16 km) earthquakes and reverse faulting for the deeper (depth > 16 km) earthquakes. We are unaware of any stress tensors analysis available in the Kumaon–Garhwal Himalaya region.

3. Data analysis

3.1. Data

We use data recorded by a temporary network of digital broadband seismic stations operated in two phases during April 2005 to June 2008 (Fig. 1). In the first phase (April 2005 to October 2006) a northeast–southwest profile (with 20 seismic stations) was operated at a spacing of ~10 km. This seismic profile was traversing the major fault systems with a few off profile stations. Later, during October 2006 to June 2008, the seismic stations were distributed in the region at a station spacing of ~50 km (details in Ashish et al., 2009; Mahesh et al., 2013). All the stations were equipped with CMG-3T/3ESP (120 s period) Guralp digital broadband sensors and 24-Bit REFTEK (RT 130-01) data recorders with 4 GB swappable hard disk and GPS. Seismic waveforms were recorded continuously at 50 samples per second.

For the present study, we select 94 well located earthquakes (Fig. 2) out of 1150 earthquakes (Fig. 2 insert) from Mahesh et al. (2013). These earthquakes recorded by at least 8 seismographs have azimuth gap less than 120° and focal depth in the range of 5 to 41 km (Fig. 3). Few earthquakes in the Gangetic plain have azimuthal gap above 120°. The average number of P- and S-arrivals is 16 and 13, respectively, for an earthquake.

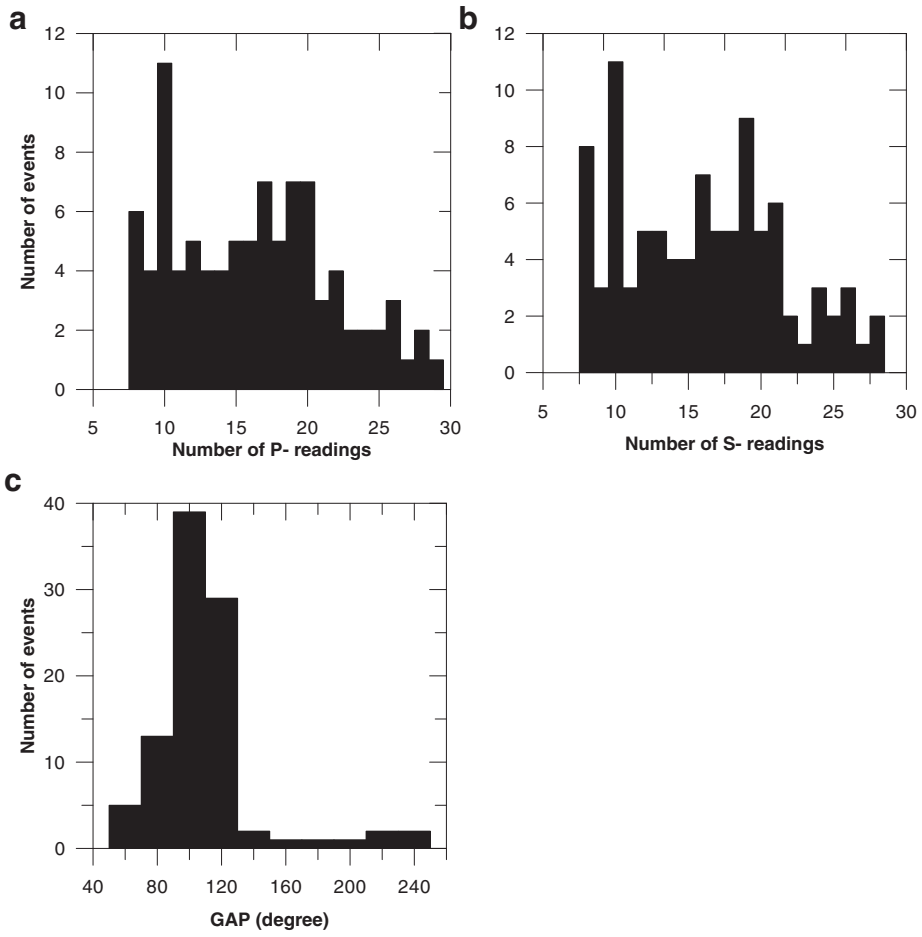

Fig. 3. Constraints on the data used for inversion. Histograms show the number of earthquakes with P-readings (a), S-readings (b), and azimuthal gap distribution (c).

3.2. Determination of fault-plane solutions

We determine fault plane solutions (FPS) of the selected 94 earthquakes (Fig. 2) using absolute amplitudes of P- and SH- (S-wave polarized in the horizontal plane) waves as well as P-wave polarities. We use the moment tensor inversion program (INVRAD) of Ebel and Bonjer (1990). In this method, theoretical amplitudes are calculated from the far-field solutions for a shear point-source dislocation in a homogeneous infinite medium, with corrections of the incident angles at the surface and geometrical spreading. The best fit solution of each earthquake is determined by minimizing the residual between the observed and theoretical amplitudes, by varying the grid for strike, dip and slip angles at 5° intervals. Fig. 4 shows the fit between the observed and calculated amplitudes for selected earthquakes. Fig. 5 shows the calculated fault plane solutions of two earthquakes by dividing observed polarities from the recorded seismograms at different seismic stations. This example shows that there are quite enough polarity measurements, by which it is possible to divide the focal sphere into compressional and dilatational quadrants.

3.3. Stress tensor analysis

To resolve the regional stress field, we invert the calculated fault plane solutions, of all 94 earthquakes, using the linear least squares approach of Michael (1984, 1987). This method gives the best fitting compressive (σ_1), intermediate (σ_2) and tensile (σ_3) stress field vectors. The method also solves the relative magnitude of the principal stresses defined by $R = (\sigma_2 - \sigma_3) / (\sigma_1 - \sigma_3)$. This inversion method is capable of using a set of single planes, one from each focal mechanism, with a priori knowledge of the true plane. Alternatively, both planes of each focal mechanism can be used in case of ambiguity. In general, the double plane criterion is safe when it is not possible to isolate a set of single planes corresponding to the true fault plane for inversion. This linear inversion combines the usual approach of making the predicted slip direction to be parallel to the observed slip direction, with a constraint on the magnitude of tangential traction. This is done to ensure that sufficient force exists to move the fault. The inversion uses bootstrap resampling (Michael, 1987) method for selecting best-fit fault plane for defining stress directions, which also provides the 95% confidence region. In this approach, we randomly pick the fault plane solutions from the entire set to create bootstrap samples and then invert these bootstrap samples (fault plane solutions).

4. Results

4.1. Fault plane solutions result

The calculated fault plane solutions of 94 well located earthquakes are presented in Fig. 6a, b, and fault plane solution parameters of these earthquakes are listed in Table 1. Some of the fault plane solutions show higher dip angles. The higher dips have also been reported earlier for a few individual earthquake fault plane solutions (e.g., Baranowaski et al., 1984; Kumar et al., 2012; Ni and Barazangi, 1984) and composite fault plane solutions (e.g., Gaur et al., 1985; Khattri et al., 1989; Valdiya, 1980); and are considered to be associated with duplexes structure in the region (Srivastava and Mitra, 1994). The directions of compressional (P axis) and the

tensional (T axis) are shown in Fig. 7. Most of the P axes are oriented in the NNE–SSW direction, the direction of the ongoing India–Eurasia collision. However, for a few normal fault mechanism, the P axes are directed in the WNW–ESE direction. Of the 94 earthquakes, 55 earthquakes are in the MCT zone, 30 earthquakes in the Lower Himalaya and 9 earthquakes are in the Gangetic plain. Fig. 6a

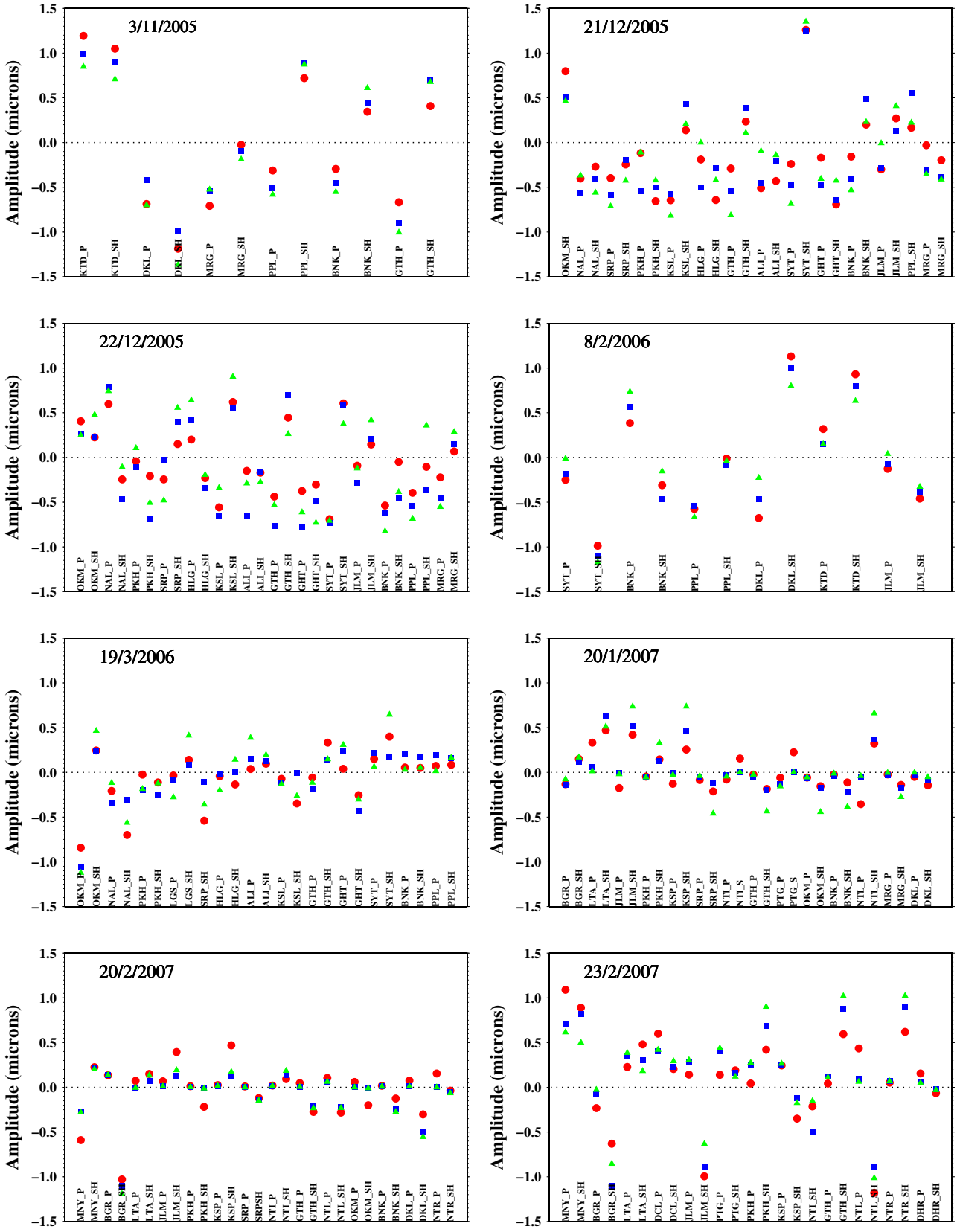

Fig. 4. Fit of observed and theoretical body-wave amplitudes, for the P- and S-amplitude inversion for focal mechanisms. Circle, triangle and square show observed amplitude, calculated moment tensor amplitude and double-couple amplitude, respectively.

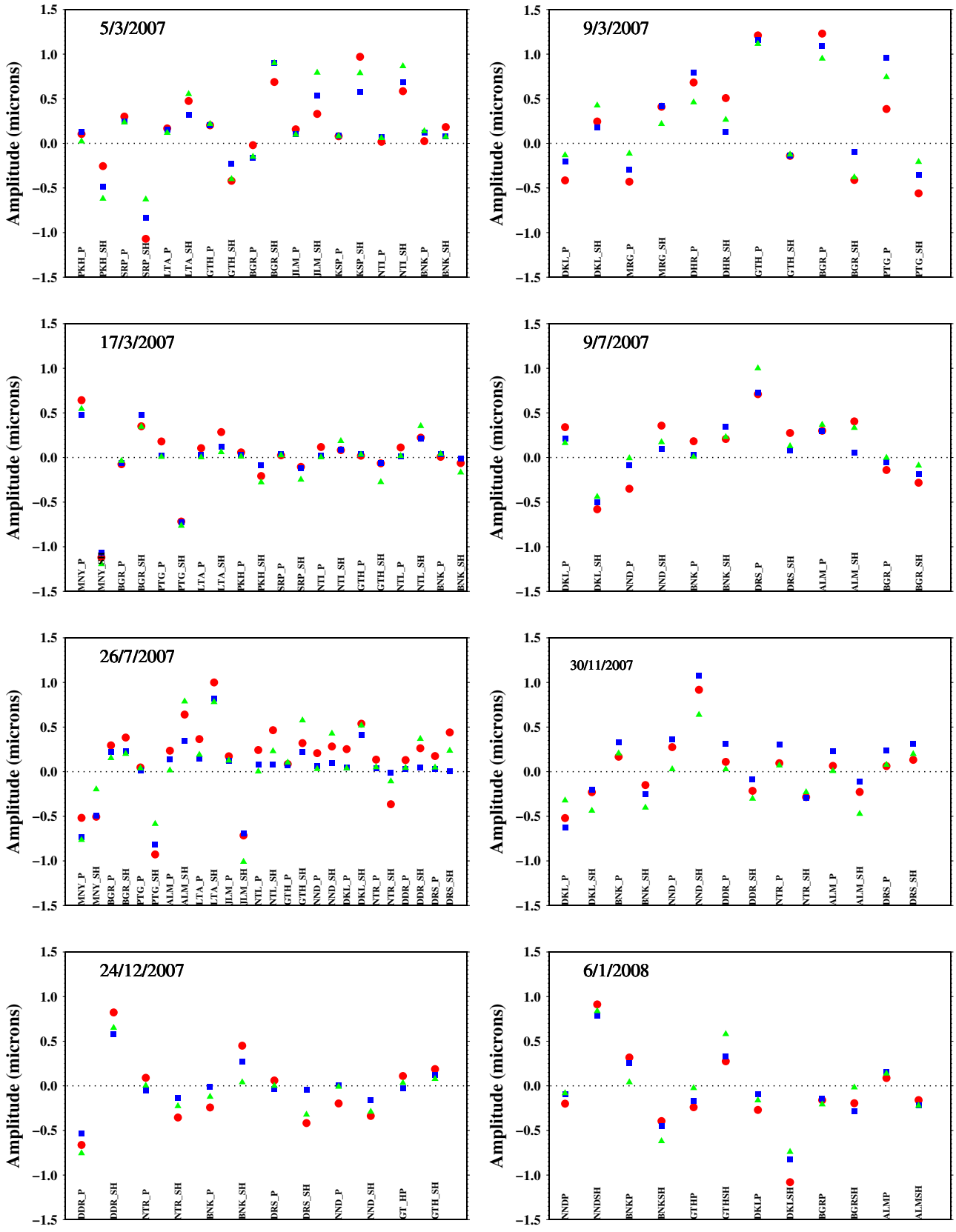

Fig. 4 (*continued*).

shows the fault plane solutions of earthquakes in the MCT zone; and Fig. 6b for the earthquakes in the Lower Himalaya and Gangetic plain. The available fault plane solutions from the global data sets (Harvard CMT Data Base, for the period 1976–2012) and one earthquake (no. 13) from Molnar and Chen (1982) are plotted in Fig. 8. The calculated fault plane solutions of two different earthquakes

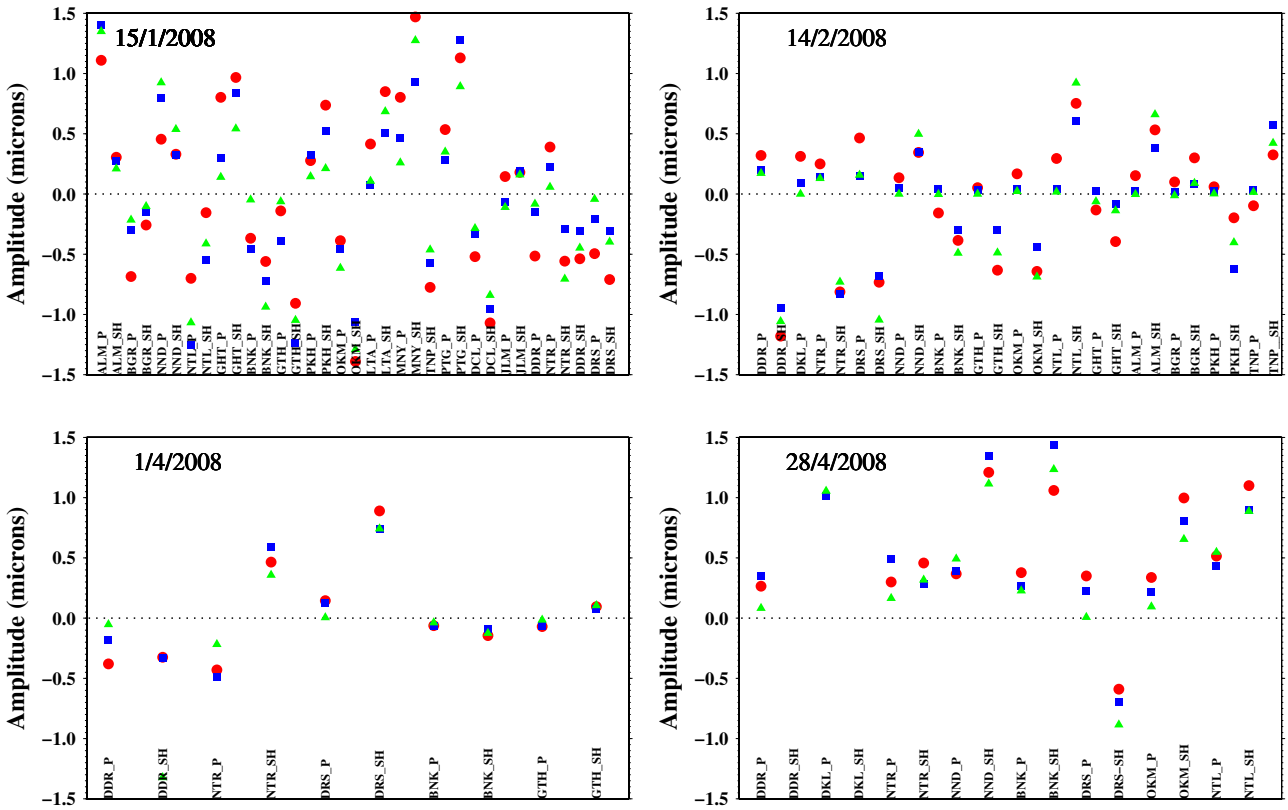

Fig. 4 (*continued*).

(4, 12 in Fig. 6a) show similar solutions as reported by Harvard CMT solutions for these earthquakes (7 and 9 in Fig. 8). This provides credence to our solutions. Majority of the earthquakes have thrust faulting, with few showing normal or strike-slip behavior.

In the MCT zone, out of 55 earthquakes, 41 are thrust, 8 normal and 6 strike-slip earthquakes (Fig. 6a). Majority of the normal earthquakes show E–W or NW–SE trending T-axis. The strike-slip earthquakes are mainly from the Munsiari region (around MNY station in Fig. 1), the

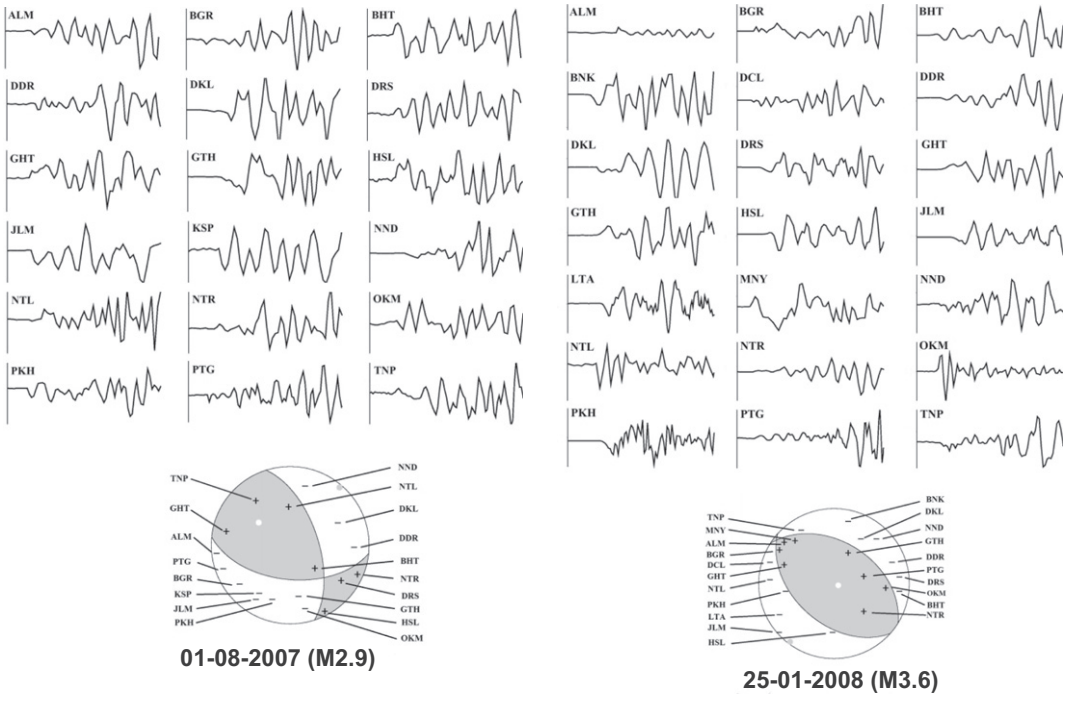

Fig. 5. Seismograms of two earthquakes, recorded at Kumaon–Garhwal Himalaya seismic stations, used to calculate fault plane solutions (below) by projecting the initial P-arrival polarities on to the lower hemisphere using equal-area projection. The plus and minus signs represent compressional and dilatational first motion, respectively.

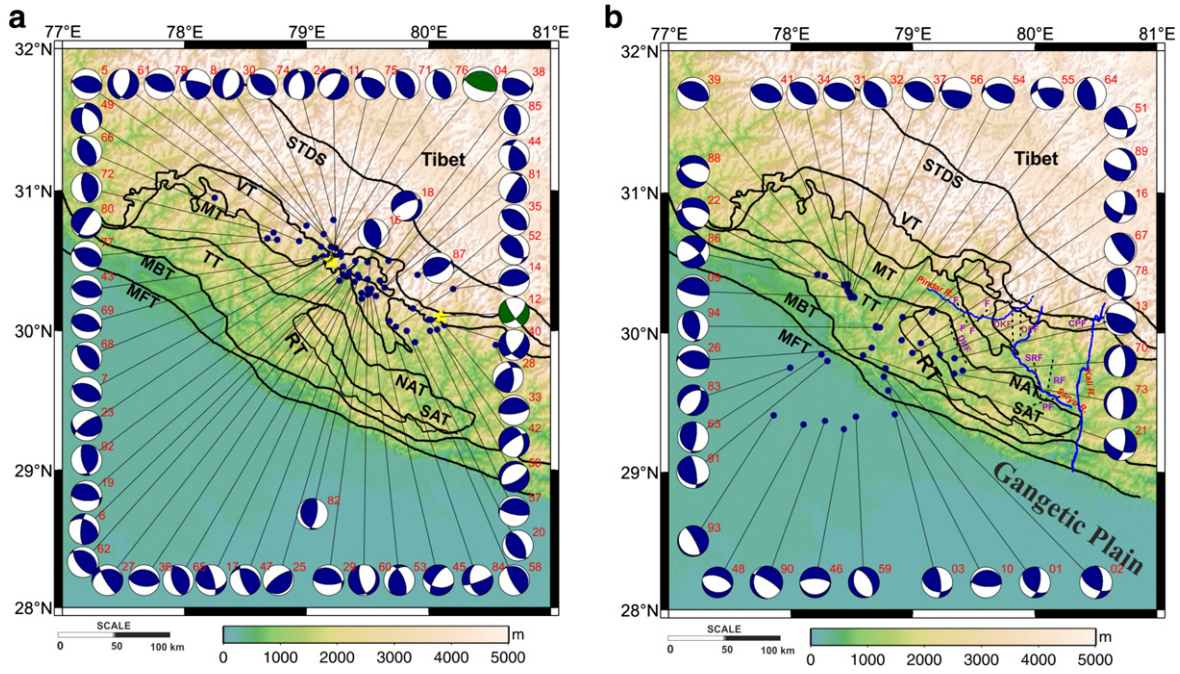

Fig. 6. Spatial distribution of fault plane solutions in different regions (a) MCT zone (b) Lower Himalaya and Gangetic plain. Green color FPSs (earthquakes shown as yellow stars) in panel A are compared with CMT solutions (earthquake nos. 7 and 9 in Fig. 8). SRF: Sarayu River Fault, RF: Ramganga Fault, DHF: Dwarhat Fault, CPF: Chipplakot Fault, DKF: Dulam–Khati Fault, DPF: Dwali Phurkiya Fault.

eastern part of study region, and with P-axes tending N–S or NE–SW. In the Lower Himalaya, out of 30 calculated fault plane solutions, 16 are thrust, 5 normal, 4 strike-slip and 5 are thrust with a strike-slip component (Fig. 6b). Majority of the thrust earthquakes in the Lower Himalaya occur near the south dipping Tons Thrust. Normal earthquakes show E–W or NE–SW trending T-axis (earthquake nos. 70, 73 and 22, 88, 89 in Fig. 6b). In the Gangetic plain, 9 fault plane solutions are determined (Fig. 6b), in which 6 fault plane solutions show normal faulting with T-axes tending NE–SW direction, nearly perpendicular to the strike of the Himalaya arc, similar to as reported by Molnar and Chen (1982) (earthquake no. 13 in Fig. 8). The remaining 3 earthquakes (3, 63, and 91), close to the Himalayan front, show thrust faulting with strike-slip component.

4.1.1. Seismic cross sections

We examine fault plane solutions along three arc-normal cross-sections AA′, BB′ and CC,′ as shown in Fig. 2. In addition to projecting the calculated fault plane solutions for the earthquakes within 20 km either side of profiles, structural geometries (modified from Célérier et al., 2009; Srivastava and Mitra, 1994) are also plotted along these cross sections (Fig. 9a, b, c). Most of the earthquakes in the Lower and Higher Himalaya show thrust mechanisms with a NNE dipping plane, similar to global studies (e.g., Molnar and Chen, 1982; Ni and Barazangi, 1984). Along the profile AA′ (Fig. 9a), two major concentrations of earthquakes occur as cluster C1: close to the MT and cluster C2: close to the TT. Most of the earthquakes in cluster C1 are in the depth range of 10–20 km and close to the northeast dipping MT. The fault plane solutions in cluster C1 are mostly of thrust type. The dip angle is steep (~42°) for the shallower earthquake and gentle (~12°) for the deeper ones. Considering the general north dipping tectonics in this part and taking north/northeasterly dipping plane as the nodal plane, the earthquakes in cluster C1 can be related with the northeast dipping MT. On the other hand, the cluster C2 falls on a southerly dipping TT. The fault plane solutions are mostly of thrust type except one shallow (~8 km depth) earthquake (no. 86, Table 1) with a strike-slip mechanism (Fig. 9a). Consider the south dipping plane as the fault plane, earthquakes in cluster C2 correlate well with the south dipping TT. The active nature of the TT has also been discussed in detail by Gupta et al. (2012). The earthquakes (83, 93 in Figs. 6b and 9a) in Gangetic plain show normal faulting, which are similar to the earlier reporting by Molnar and Chen (1982) and Ni and Barazangi (1984).

Along the profile BB′ (Fig. 9b), a cluster C3 is observed below the MT and another cluster C4 between the MBT and MT. Both the clusters show north dipping trend in the seismicity. The fault plane solutions of the selected earthquakes in cluster C3 dominantly show thrusting with a few solutions having strike-slip component. One of the nodal planes of the obtained solutions in cluster C3 is north-easterly dipping and can be correlated with the MT. Of the four fault plane solutions from cluster C4, three show dominant thrust faulting and one strike-slip. Fault plane solutions of three deeper earthquakes 18, 21 and 89, below the MHT, show normal/normal with strike-slip faulting. Four deeper earthquakes in the Gangetic plain (46, 48, 59 and 90) show normal faulting as observed along the profile AA′ (Fig. 9a).

Along the profile CC′ (Fig. 9c), the majority of the recorded earthquakes (i.e., cluster C5) are on the NE dipping MT. Most of the calculated fault plane solutions of cluster C5 indicate thrust mechanism with NE dipping plane. Three earthquakes (12, 40 and 84 in Figs. 6a and 9c) in cluster C5, show strike-slip faulting. Among these, the fault plane solution of one earthquake (01/02/2006, M 4.8; number 12 in Fig. 6a) has a similar solution as reported by the Harvard CMT catalog (earthquake no. 9 in Fig. 8). It may be noted that these three earthquakes are clustered around 8–15 km depth within foot wall of the Munsiari Thrust as well as north of the NAT (Fig. 6a). Fault plane solutions for three earthquakes (70, 73 and 78), to the north of MBT and close to the MHT, are also obtained. The earthquakes 70 and 73 show normal faulting and the earthquake 78 shows reverse faulting with strike-slip component. The earthquake (03), to the south of the MFT, shows strike-slip faulting, which is similar with the global solutions in this region (e.g., Molnar and Chen, 1982; Ni and Barazangi, 1984).

4.2. Stress Inversion results

Fig. 10 shows the results of stress inversion using both the planes of each focal mechanism. The stress model in the MCT zone, after the

Table 1
Parameters of the calculated fault plane solutions.

S. no	Date yr/mn/dy	Origin time hr:min:sec	Latitude (°N)	Longitude (°E)	Depth (km)	Nodal plane 1			Nodal plane 2			
						Strike (°)	Dip (°)	Rake (°)	Strike (°)	Dip (°)	Rake (°)	Mag.
1	2005/07/11	21:05:22.08	29.69	78.76	22.30	129	47	37	12	64	131	1.7
2	2005/11/03	02:06:49.10	29.75	78.78	26.68	118	57	41	3	57	139	1.6
3	2005/11/20	08:36:26.87	29.42	78.85	20.00	107	40	29	354	72	126	2.5
4	2005/12/14	07:09:50.40	30.50	79.20	14.00	270	25	70	112	67	99	5.3
5	2005/12/21	23:39:47.09	30.60	79.13	16.70	263	45	79	98	46	101	2.8
6	2005/12/22	01:37:31.57	30.36	79.27	20.00	185	62	126	308	44	42	2.5
7	2005/12/22	18:26:32.56	30.54	79.25	17.10	115	44	93	291	46	87	2.0
8	2005/12/24	00:44:02.74	30.69	79.14	20.00	171	40	156	280	75	53	1.6
9	2006/01/03	11:57:38.38	30.26	78.52	21.30	275	15	82	103	75	92	1.7
10	2006/01/10	22:50:09.07	29.59	78.80	36.60	256	23	73	94	68	97	1.6
11	2006/01/14	13/30/42.69	30.59	79.24	16.60	253	31	−51	30	66	−111	2.0
12	2006/02/01	22:24:11.30	30.15	80.10	14.00	48	60	−16	146	76	−149	4.8
13	2006/02/08	12:11:05.14	29.82	79.34	29.39	290	70	81	135	22	113	3.0
14	2006/02/14	19:17:28.00	30.30	80.20	38.60	82	62	90	262	28	90	4.3
15	2006/03/24	14:04: 2.61	30.30	79.50	11.00	157	40	80	350	51	98	2.8
16	2006/05/01	00:37:52.64	29.93	79.07	18.80	116	59	−154	12	68	−34	2.5
17	2006/05/16	03:45:10.35	30.35	79.39	15.50	093	38	22	345	77	126	3.8
18	2006/05/26	04:13:19.50	30.49	79.50	39.10	244	70	−70	17	28	−133	3.3
19	2006/05/30	07:46:01.20	30.50	79.40	12.00	93	65	72	311	30	124	2.7
20	2006/05/30	18:25:29.69	29.92	79.89	13.00	140	32	80	332	59	96	2.6
21	2006/06/16	08:58:35.58	29.84	78.59	35.54	115	59	−153	10	67	−34	2.0
22	2006/06/19	23:56:57.07	30.42	78.22	20.00	144	45	−52	276	56	−122	2.2
23	2006/06/30	01:33:20.39	30.49	79.16	16.50	231	72	63	110	32	144	2.4
24	2006/07/31	08:15:11.18	30.79	79.22	16.50	211	37	−54	349	61	−114	2.8
25	2006/09/16	19:30:54.10	30.27	79.45	15.10	45	17	82	233	73	92	2.0
26	2006/09/24	02:17:58.08	29.90	78.66	19.26	267	36	70	111	56	104	2.5
27	2006/09/24	21:52:56.80	30.42	79.35	14.20	255	31	20	148	80	119	2.8
28	2006/09/26	04:04:22.80	29.90	80.55	46.00	356	61	−48	114	49	−140	4.4
29	2006/10/05	19:17:58.22	30.37	79.50	06.30	56	18	121	204	75	80	2.0
30	2006/11/07	10:59:32.52	30.53	79.28	06.00	29	31	−72	188	61	−101	3.0
31	2007/01/01	01:54:16.11	30.29	78.48	12.00	107	53	90	287	37	90	1.6
32	2007/01/04	02:11:16.01	30.29	78.48	16.00	142	35	90	323	55	90	1.6
33	2007/01/18	17:51:29.10	30.04	80.13	09.00	269	18	96	83	72	88	2.7
34	2007/01/20	13:48:01.03	30.31	78.47	15.65	126	50	90	306	40	90	1.5
35	2007/01/20	23:19:21.61	30.16	79.87	20.00	216	50	90	36	40	90	1.9
36	2007/02/02	05:09:52.35	30.40	79.34	13.60	97	57	90	277	33	90	2.7
37	2007/02/03	02:09:13.60	30.27	78.49	13.50	118	60	90	298	30	90	1.7
38	2007/02/05	16:50:42.62	30.56	79.67	08.00	81	37	62	295	58	109	2.7
39	2007/02/14	14:00:19.03	30.35	78.43	19.00	113	61	90	293	29	90	1.8
40	2007/02/20	17:34:41.96	30.08	80.02	08.70	153	54	−147	42	64	−41	2.0
41	2007/02/24	02:01:51.42	30.33	78.46	17.12	108	48	90	288	42	90	1.7
42	2007/02/23	09:15:00.35	30.08	80.00	05.00	236	72	−58	352	36	−148	2.3
43	2007/03/01	08:41:27.48	30.52	79.07	13.00	280	37	87	104	53	92	2.4
44	2007/03/03	02:26:54.24	30.25	79.57	16.00	307	48	38	189	63	131	2.7
45	2007/03/05	06:48:01.12	30.30	79.53	18.00	101	50	−30	211	67	−136	2.2
46	2007/03/09	05:35:38.07	29.31	78.44	24.10	87	20	−94	271	70	−89	2.1
47	2007/03/17	10:04:55.70	30.38	79.43	14.00	290	28	43	161	71	111	3.8
48	2007/07/09	19:48:35.11	29.34	78.10	21.50	97	34	−100	289	57	−83	2.5
49	2007/07/22	23:02:13.50	30.95	78.25	24.90	181	63	−56	305	42	−138	4.9
50	2007/07/26	21:17:28.51	30.01	80.07	12.00	226	27	−103	61	64	−83	2.4
51	2007/08/01	21:16:40.67	29.95	78.91	15.50	96	54	37	342	61	138	2.9
52	2007/08/14	12:58:13.39	30.03	79.73	13.00	336	43	122	115	55	64	2.8
53	2007/08/18	07:14:44.86	30.27	79.52	13.50	210	37	138	336	66	61	2.6
54	2007/10/06	11:08:43.08	30.05	78.70	17.10	267	39	61	122	57	111	2.5
55	2007/10/06	11:44:57.20	30.04	78.73	08.00	264	60	43	149	54	142	3.1
56	2007/10/07	05:28:45.27	30.26	78.49	22.15	277	74	−80	64	19	−121	2.8
57	2007/10/29	11:06:42.50	30.00	80.01	06.00	252	19	62	101	73	99	2.2
58	2007/10/30	01:21:23.00	30.00	79.82	12.70	309	15	67	153	76	96	3.1
59	2007/11/30	21:55:21.27	29.40	78.54	19.31	162	35	−78	327	56	−98	1.9
60	2007/12/12	06:33:10.80	30.26	79.50	11.00	23	26	−55	165	69	−106	2.3
61	2007/12/18	16:58:53.28	30.75	79.00	09.00	163	35	−119	17	60	−71	2.1
62	2007/12/20	21:03:43.95	30.40	79.30	16.00	300	29	70	143	63	101	2.0
63	2007/12/24	18:46:43.89	29.85	78.25	22.10	147	21	49	10	74	104	1.5
64	2007/12/26	09:01:13.91	30.12	78.92	20.00	182	24	108	342	67	82	1.9
65	2008/01/01	20:34:27.81	30.48	79.42	19.00	332	32	82	161	58	95	2.1
66	2008/01/04	06:59:05.69	30.64	78.94	10.70	166	42	104	327	50	78	2.0
67	2008/01/06	15:43:55.33	29.86	79.00	04.01	143	79	85	348	12	114	1.7
68	2008/01/12	16:31:23.76	30.54	79.20	08.00	311	32	78	145	59	97	2.4
69	2008/01/15	04:49:41.51	30.53	79.14	13.10	298	42	104	99	50	78	2.2
70	2008/01/15	13:15:19.67	29.73	79.40	15.70	199	28	−70	357	64	−100	2.4
71	2008/01/16	05:20:30.46	30.54	79.19	12.60	327	40	81	159	51	97	3.0
72	2008/01/16	21:31:07.61	30.70	78.73	10.80	170	66	90	350	24	90	2.1
73	2008/01/20	20:41:45.52	29.71	79.34	18.70	199	17	−71	359	74	−96	2.1
74	2008/01/25	15:24:23.82	30.60	79.20	16.30	302	44	83	130	46	97	3.6

Table 1 (*continued*)

S. no	Date yr/mn/dy	Origin time hr:min:sec	Latitude (°N)	Longitude (°E)	Depth (km)	Nodal plane 1			Nodal plane 2			
						Strike (°)	Dip (°)	Rake (°)	Strike (°)	Dip (°)	Rake (°)	Mag.
75	2008/01/25	21:29:37.20	30.52	79.20	11.00	285	56	53	158	49	132	2.9
76	2008/01/25	23:59:04.63	30.49	79.18	12.00	331	40	80	164	51	98	2.4
77	2008/01/26	10:51:08.10	30.65	78.76	16.00	285	43	73	128	49	105	2.4
78	2008/01/28	03:14:01.93	29.85	79.22	19.95	132	36	47	1	65	116	1.9
79	2008/01/28	16:55:47.65	30.56	79.28	17.00	289.	35	89	110	55	91	2.1
80	2008/01/30	20:50:41.48	30.66	78.68	41.00	91	17	−32	212	81	−105	2.2
81	2008/02/07	22:24:52.13	30.31	79.64	08.60	339	19	38	213	78	105	1.8
82	2008/02/10	13:28:14.62	30.23	79.45	14.00	160	25	60	12	69	103	2.1
83	2008/02/14	20:12:03.21	29.75	78.00	29.51	239	44	−61	21	53	−115	1.6
84	2008/03/14	01:15:08.06	30.07	79.68	15.00	170	48	−165	70	79	−43	1.8
85	2008/03/20	00:43:54.43	30.36	79.60	17.00	164	37	82	354	53	96	2.4
86	2008/04/01	21:43:19.89	30.35	78.47	07.62	312	70	−30	53	62	−157	1.7
87	2008/04/14	17:45:53.02	30.14	79.91	18.80	274	31	120	60	64	73	2.1
88	2008/04/17	19:45:19.97	30.41	78.28	08.00	125	51	−63	266	46	−119	2.6
89	2008/04/22	23:29:31.81	30.15	79.16	35.00	348	35	−35	108	71	−120	2.3
90	2008/04/27	15:32:43.45	29.37	78.21	44.70	176	23	−37	301	76	−109	1.9
91	2008/04/28	19:51:03.75	29.80	78.30	21.96	111	27	34	350	75	113	1.6
92	2008/05/25	15:24:08.20	30.46	79.30	32.00	25	30	126	165	66	71	2.5
93	2008/06/10	16:27:50.83	29.41	77.86	29.48	129	10	−112	331	81	−86	2.0
94	2008/06/11	23:00:59.35	30.04	78.70	07.00	151	39	69	357	54	106	2.4

inversion of 55 fault plane solutions and with 95% confidence limit, shows well constrained σ_1 and σ_3 (Fig. 10a). The inversion results show average misfit of 10.5° and stress magnitude R = 0.5 with azimuth and plunge of N220° and N004° (for σ_1), N305° and N011° (for σ_2); and N112° and N078° (for σ_3) (Fig. 10a and Table 2). The principle compressive stress (σ_1) is oriented NNE–SSW, consistent with the direction of the ongoing India–Eurasia collision (Fig. 10a). The inversion of 30 fault plane solutions in the Lower Himalaya gives a relatively larger spread of σ_1 and σ_3, with 95% confidence limits. The inversion results show an average misfit of 14.5° and R = 0.6. The maximum principal stress axis (σ_1) trends N199° and the minimum principal stress (σ_3) trends N097° (Fig. 10b and Table 2). Although the σ_1 is oriented NNE–SSW, like that in the MCT zone, the larger spread in 95% confidence limits for σ_1 and σ_3 indicates that the stress field is not homogeneous, possibly due to several local faults in the Lower Himalaya (Valdiya, 1980) (Fig. 1).

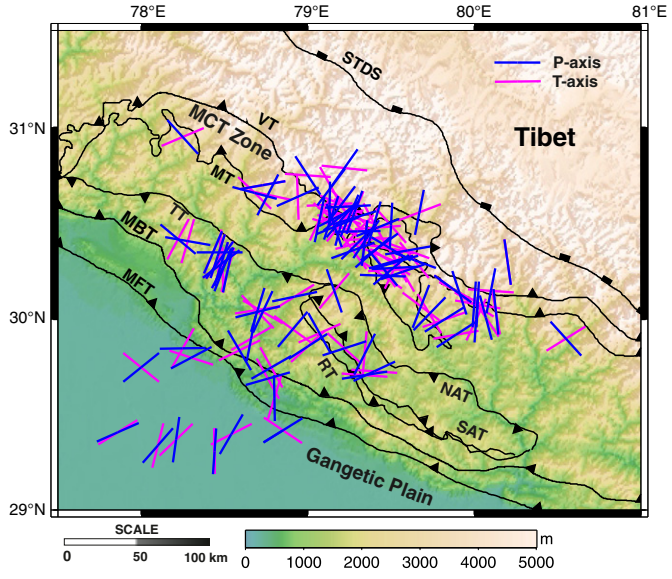

Fig. 7. P axis and T axis distributions of calculated fault plane solutions.

In the Gangetic plain, inversion of 6 fault plane solutions, with 95% confidence limits, shows a large spread of σ_1 and σ_3 (Fig. 10c). The average misfit for best-fitting stress model is 8.5°, which is low value, and can be due to small number of fault plane solutions used in inversion. The maximum principal stress axis (σ_1) trends N168° and minimum principal stress axis (σ_3) trends N062° (Fig. 10c and Table 2). The maximum principal stress axis is N–S directed and near vertical, which can be attributed to the flexing of the Indian plate.

5. Discussion

The calculated fault plane solutions of the 94 well located earthquakes in Kumaon–Garhwal Himalaya are mix of thrust, normal and strike-slip mechanism. Spatially, the thrust earthquakes are mostly in the MCT zone and in the Lower Himalaya. In general, the maximum compressive stress (σ_1) is oriented in the NNE–SSW direction, correlating with the prevailing stress condition due to northward movement of Indian plate. Most of the thrust earthquakes are in the depth range of 8–22 km, and follow the MT and TT at depth. The dip angle varies from steeper to gentle, with increasing depth, indicating the listric nature of the MT and TT. The observed thrust earthquakes in the Lower Himalaya can be due to interseismic strain accumulation on the MHT (Pandey et al., 1995) or due to blind thrust related to fault propagation fold (Thakur, 2004). Although the Himalayan collision tectonics is dominated by thrust type earthquakes, we obtain good number of normal and strike-slip earthquakes possibly related with the local structure and/or regional Himalayan tectonics.

The strike-slip earthquakes to the south of the MT (12, 40, 45 and 84 in Fig. 6a) are observed near the Munsiari region, the eastern part of the Kumaon Himalaya (and western side of the Nepal Himalaya). In the past, this region has experienced strong to major earthquakes in 1916 (M 7.0) and 1954 (M 6.2). Composite fault plane solution of the earthquakes in this region shows strike-slip type mechanism (Paul et al., 2010). Two earthquakes of 1966 (M 5 and M 7) in the Nepal Himalaya, further east to the Munsiari region, also show strike-slip mechanism (Paul et al., 2010). The obtained strike-slip earthquake mechanism, in the Munsiari region, can be associated with the Dwali Phurkiya strike-slip Fault (DPF, Fig. 6b) mapped using morphometric analysis (Kothyari, 2014), or with the Chiplakot strike-slip fault (CPF, Fig. 6b), which is responsible for a large number of earthquakes in this region. The fault is geologically mapped to the east of this region along the Kali River valley (Paul, 1985). The presence of strike-slip fault(s) in

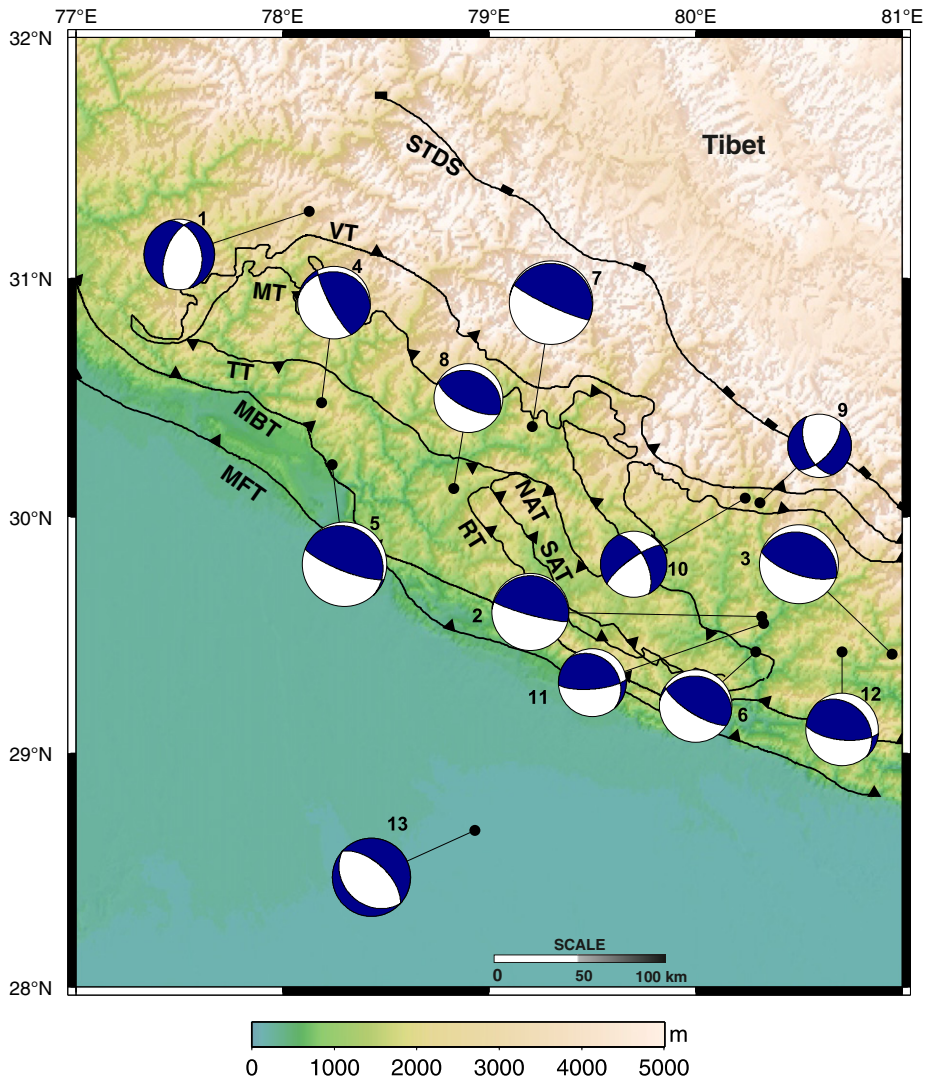

Fig. 8. Map view of the FPSs, from global data sets: CMT catalog (Harvard CMT Data Base) during 1976 to 2012, and Molnar and Chen, 1982 (earthquake no. 13).

this region has also been suggested through lateral deflections of the Kali and Saryu rivers (Fig. 6b), which are related with the active strike-slip fault movement on strike-slip fault(s) in this region (Kothyari, 2014; Paul et al., 2010; Valdiya, 1976). Based on observed seismicity to the south of the MCT, Thakur (2004) infers the strike-slip fault in the steep upper part of an active blind listric thrust, which is an active splay of the Munsiari Thrust and suggested to be associated with the fault bent or fault propagation fold below the Lower Himalaya. Further, Dubey and Bhat (1986) explain the conjugate strike-slip faulting, across the thrust in this region, with the locking of the thrust fault due to steepening of the thrust surface. Earthquakes 16 and 86 (Fig. 6b) can be related with some local transverse structures in this collision environment.

The normal earthquake (no. 50, Fig. 6a) in the Kumaon Himalaya and showing NW–SE (arc parallel) extension can be related with the Dulam–Khati Fault (DKF, Fig. 6b), in the Pindar river basin of this region, as mapped by Kothyari (2014). Alternatively, this earthquake along with other earthquakes (11, 18, 42; Fig. 6a), also showing NW–SE (arc-parallel) extension in the MCT zone of Garhwal Himalaya, can be linked with southward migration of the active thrust zone in the radial expansion model proposed for this region (Hintersberger et al., 2010, 2011; Murphy et al., 2009). Hintersberger et al. (2010, 2011) observes that the NW–SE oriented extension is pronounced in the vicinity of the thrust belt and mainly up to MCT zone.

Unlike the normal earthquakes with arc-parallel extension occurring mainly up to MCT zone, the normal earthquakes with NE–SW (arc-normal) extension are observed further south of the MCT zone and in the Lower Himalaya (earthquakes 22, 88, 89; Fig. 6b). Close to earthquakes 22 and 88, the Ghansali earthquake (Mw 4.1, 3 May 2010) also shows normal type of mechanism with N–S extension (Kumar et al., 2014). The earthquake 89, near the SAT (Fig. 6b), can be related to transverse faults, which are reported to be neo-tectonically active (Goswami and Pant, 2008). Similarly, other earthquakes (22, 88; Fig. 6b) with arc-normal extension can be due to local transverse structures developed in this compressive regime. Otherwise, arc-normal extension in this region can be explained by reactivation of the reverse faults in this region (Hintersberger et al., 2011) or by localized extension on the foot wall of the MCT (Searle et al., 2008).

The normal faults with E–W extension (24, 30, 61, 70, 73; Fig. 6a, b) are observed in the Higher and Lower Himalaya. Active E–W extension both in the internal parts of Himalaya and Tethyan region has been indicated in geodetic measurements (Banerjee and Burgmann, 2002; Jade et al., 2014) and fault kinematic study (Hintersberger et al., 2010, 2011). Following Hintersberger et al. (2010, 2011), we believe that the E–W extension in this region can be related with (1) the ongoing extensional tectonics in the adjacent Tibet region and the similar extensional tectonics is possibly extending into internal part of the Himalaya; or (2) the transferred E–W extension from the Tibet Plateau into the

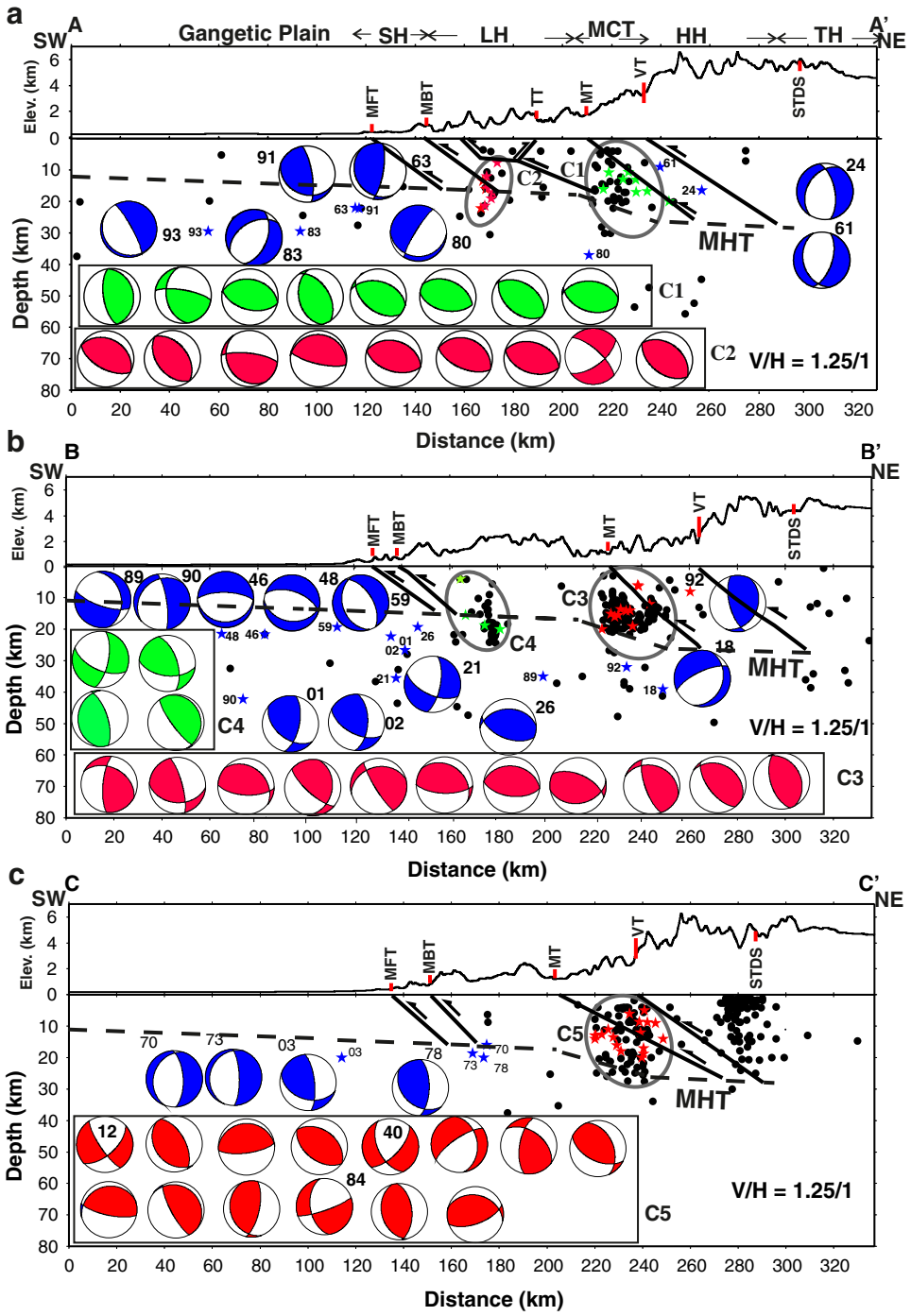

Fig. 9. (a, b, c): The calculated fault plane solutions of the earthquakes (within 20 km either side of respective profile) along three arc-normal cross-sections AA′, BB′ and CC′ (as shown in Fig. 2). The structural cross-sections are re-drawn from (a) Srivastava and Mitra (1994) and (b) and (c) Célérier et al. (2009). The FPSs with different colors (red, green and blue) correspond to earthquakes with respective color stars. C(1–5) are the clusters discussed in the text. Filled circles are the earthquakes (Mahesh et al., 2013), within 20 km either side of respective profile. The MHT configuration is taken from Caldwell et al. (2013).

Himalaya, where the Karakorum fault is not decoupling the normal faulting on either side of it. However, in the complex Himalaya region, the presence of any local structure, which can be responsible for E–W extension, cannot be ruled out.

The normal faulting in the Gangetic plain, however, can be explained by flexure of the Indian plate beneath the Himalaya as suggested in earlier studies (Molnar and Chen, 1982; Ni and Barazangi, 1984).

The large number of fault plane solutions provided here for the Kumaon–Garhwal Himalaya, a proposed potential zone for future great earthquake(s), can provide useful information to synthesize the more detailed seismotectonic model for this region and can be useful for seismic hazard investigations. The stress inversion results show that the maximum compressive stress (σ_1) in the Kumaon–Garhwal Himalaya is near horizontal, and NNE–SSW directed; consistent with the northward movement of the Indian plate that continues to push the Eurasian plate. In the Gangetic plain the N–S directed and near vertical compressive stress (σ_1) can be explained by flexure of the Indian plate to the south.

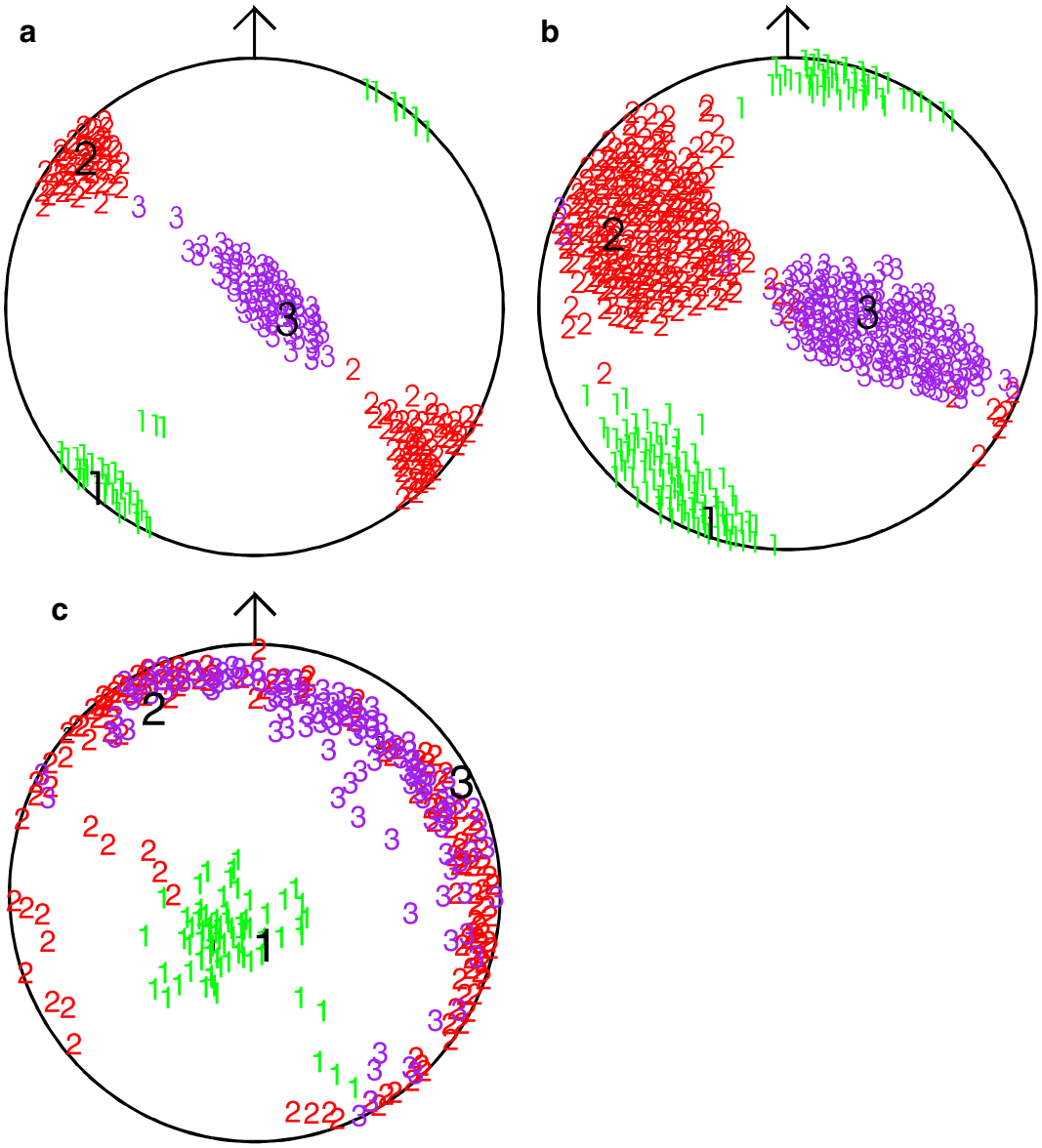

Fig. 10. Stress inversion results obtained in (a) MCT zone, (b) Lower Himalaya, and (c) Gangetic plain. The cluster numbers in each circle comprises the individual estimates of the principle compressive (σ_1), intermediate (σ_2) and tensile (σ_3) stress axis orientations.

6. Conclusions

The fault plane solutions of the 94 well located earthquakes in the Kumaon–Garhwal Himalaya reveal a majority of thrust earthquakes, and a number of normal and strike-slip earthquakes as well. Most of the thrust earthquakes are in the MCT zone and in the Lower Himalaya. In depth, the thrust earthquakes occur at or above the MHT, and follow the MT and TT. The strike-slip earthquakes are mainly observed in the Lower Himalaya as well as around the Munsiari region (proximity of Nepal Himalaya) in the MCT zone. The normal earthquakes with arc-normal (NE–SW), arc-parallel (NW–SE) and E–W extension are observed in different parts of the Kumaon–Garhwal Himalaya. The normal earthquakes, related with the flexure of the Indian plate are observed in the Gangetic plain. The stress inversion results show that the compressive stress is near horizontal and NNE–SSW directed in the Kumaon–Garhwal Himalaya; and near vertical in the Gangetic plain. The observed seismicity identifies various localized zones of stress accumulation; and calculated fault plane solutions clearly show varying deformation styles in the Kumaon–Garhwal Himalaya. The result presents new data set emphasizing a need for further detailed knowledge of local structures along with regional tectonics, through long term multi-disciplinary studies for improved understanding of the active seismotectonics in this seismically vulnerable region.

Table 2
Stress tensor directions estimated from focal mechanism solutions in different regions.

Region	σ1 (°) (pl, az)	σ_2 (°) (pl, az)	σ_3 (°) (pl, az)	R	Avg. misfit (°)
MCT zone	220, 4	305, 11	112, 78	0.5	10.5
Lower Himalaya	199, 6	291, 26	97, 63	0.6	14.5
Gangetic plain	168, 72	331, 17	62, 5	0.4	8.5

Acknowledgments

PM was supported by research fellowship from CSIR, India to pursue his Ph.D. SSR is supported by JC Bose fellowship grant from the DST, New Delhi. The results presented are part of the research project (DST/MMS-2/SU/2003) supported by the Department of Science

and Technology (DST), New Delhi. Part of the work was supported by the CSIR-NGRI projects (MLP-6505 and PSC-0204). Dr. G.C. Kothyari is thanked for useful discussion. Prof. Jean-Philippe Avouac and Prof. Mian Liu (the editors), two anonymous reviewers and Dr. Kusala Rajendran are sincerely thanked for their valuable suggestions for improving the quality of the manuscript significantly.

References

Ambraseys, N., Jackson, D., 2003. A note on early earthquakes in northern India and southern Tibet. Curr. Sci. 84, 571–582.
Ashish, Padhy, A., Rai, S.S., Gupta, S., 2009. Seismological evidence for shallow crustal melt beneath the Garhwal High Himalaya, India: implications for Himalayan channel flow. Geophys. J. Int. 177 (1), 1111–1120.
Avouac, J.P., 2003. Mountain building, erosion and the seismic cycle in the Nepal Himalaya. Adv. Geophys. 46, 1–80.
Avouac, J.P., 2007. Dynamic processes in extensional and compressional settings—mountain building: from earthquakes to geological deformation. In: Schubert, G. (Ed.), Treatise on Geophysics. Elsevier, Amsterdam, pp. 377–439.
Banerjee, P., Burgmann, R., 2002. Convergence across the northwest Himalaya from GPS measurements. Geophys. Res. Lett. 29 (13), 31–34.
Baranowaski, J., Armbuster, J., Seeber, L., 1984. Focal depths and fault plane solutions of earthquakes and active tectonics of the Himalaya. J. Geophys. Res. 89 (B8), 6918–6928.
Basse, J., Courtillot, V., Pozzi, J.P., Westphal, M., Zhou, Y.X., 1984. Paleomagnetic estimates of crustal shortening in the Himalayas thrusts and Zangbo suture. Nature 311, 621–626.
Berger, A., Jouanne, F., Hassani, R., Mugnier, J.L., 2004. Modelling the spatial distribution of present-day deformation in Nepal: how cylindrical is the Main Himalayan Thrust in Nepal? Geophys. J. Int. 156, 94–114.
Bilham, R., Bodin, P., Jackson, M., 1995. Entertaining a great earthquake in Western Nepal: historic inactivity and geodetic test for the development of strain. J. Nepal Geol. Soc 11, 73–88 (Special Issue).
Bilham, R., Gaur, V.K., Molnar, P., 2001. Himalayan seismic hazard. Science 293, 1442-1442.
Caldwell, W.B., Klemperer, S.L., Lawrence, J.F., Rai, S.S., Ashish, 2013. Characterizing the Main Himalayan Thrust in the Garhwal Himalaya, India with receiver function CCP stacking. Earth Planet. Sci. Lett. 367, 15–27.
Célérier, J., Harrison, T.M., Webb, A.A.G., Yin, A., 2009. The Kumaun and Garwhal Lesser Himalaya, India. Part 1: structure and stratigraphy. Geol. Soc. Am. Bull. 121 (9–10), 1262–1280. http://dx.doi.org/10.1130/B26344.1.
DeCelles, P.G., Robinson, D.M., Quade, J., Ojha, T.P., Garzione, C.N., Copeland, P., Upreti, B.N., 2001. Stratigraphy, structure, and tectonic evolution of the Himalayan fold–thrust belt in western Nepal. Tectonics 20 (4), 487–509.
Dubey, A.K., Bhat, M.I., 1986. The role of reactivation of pre-rift basement listric faults in the structural evolution of the Himalaya: an experimental study. In: Saklani (Ed.), Himalayan Thrusts and Associated Rocks, Current Trends in Geology 9, pp. 265–290.
Ebel, J.E., Bonjer, K.P., 1990. Moment tensor inversion of small earthquakes in southwestern Germany for the fault plane solution. Geophys. J. Int. 101, 133–146.
Gahalaut, V.K., 2008. Major and great earthquakes and seismic gaps in the Himalayan arc. Geol. Soc. India Mem. 66, 373–393.
Gaur, V.K., Chander, R., Sarkar, I., Khatri, K.N., Sinvhal, H., 1985. Seismicity and the state of stress from investigations of local earthquakes in the Kumaun Himalaya. Tectonophysics 118, 243–251.
Goswami, P.K., Pant, C.C., 2008. Morphotectonic evolution of the Binau–Ramganga–Naurar transverse valley, southern Kumaun Lesser Himalaya. Curr. Sci. 94 (12), 1640–1645.
Gupta, S., Mahesh, P., Sivaram, K., Rai, S.S., 2012. Active fault beneath the Tehri dam, Garhwal Himalaya — seismological evidence. Curr. Sci. 103 (11), 1343–1347.
Hintersberger, E., Thiede, R.Ch., Strecker, M.R., Hacker, B.R., 2010. East–West extension in the NW Indian Himalaya. Geol. Soc. Am. Bull. 122, 1499–1515.
Hintersberger, E., Thiede, R.Ch., Strecker, M.R., 2011. The role of extension during brittle deformation within the NW Indian Himalaya. Tectonics 30, TC3012. http://dx.doi.org/10.1029/2010TC002822.
Jade, S., Mukul, M., Gaur, V.K., Kumar, K., Shrungeshwar, T.S., Satyal, G.S., Dumka, R.K., Saigeetha, J., Ananda, M.B., Kumar, D.P., Banerjee, S., 2014. Contemporary deformation in the Kashmir–Himachal, Garhwal and Kumaon Himalaya: significant insights from 1995–2008 GPS time series. J. Geod. 88, 539–557.
Kayal, J.R., 1996. Precursor seismicity, foreshocks and aftershocks of the Uttarkashi earthquake of October 20, 1991 at Garhwal Himalaya. Tectonophysics 263, 339–345.
Kayal, J.R., 2001. Microearthquake activity in some part of the Himalaya and the tectonic model. Tectonophysics 339, 331–351.
Kayal, J.R., Ram, S., Singh, O.P., Chakraborty, P.K., Karunakar, G., 2003. Aftershocks of the March 1999 Chamoli earthquake and seismotectonic structure of the Garhwal Himalaya. Bull. Seismol. Soc. Am. 93, 109–117.
Khattri, K.N., 1992. Local seismic investigations in Garhwal–Kumaon Himalaya. Geol. Soc. India Mem. 23, 45–66.
Khattri, K.N., Chander, R., Gaur, V.K., Sarkar, I., Kumar, S., 1989. New seismological results on the tectonics of the Garhwal Himalaya. Proc. Indian Acad. Sci. 98, 91–109.
Kothyari, G.C., 2014. Morphometric analysis of tectonically active Pindar and Saryu River basins: Central Kumaun Himalaya. Z. Geomorphol. http://dx.doi.org/10.1127/zfg/2014/0162.
Kumar, S., Wesnousky, S.G., Rockwell, T.K., Briggs, R.W., Thakur, V.C., Jayangondaperumal, R., 2006. Paleoseismic evidence of great surface-rupture earthquakes along the Indian Himalaya. J. Geophys. Res. 111, B03304. http://dx.doi.org/10.1029/2004JB003309.
Kumar, N., Paul, A., Mahajan, A.K., Yadav, D.K., Borah, Chandan, 2012. The Mw 5.0 Kharsali, Garhwal Himalayan earthquake of 23 July 2007: source characterization and tectonic implications. Current Science 102 (2), 1674–1682.
Kumar, R., Gupta, S.C., Kumar, A., 2014. Determination and identification of focal mechanism solutions for Himalayan earthquakes from waveform inversion employing ISOLA software. Nat. Hazards. http://dx.doi.org/10.1007/s11069-014-1540-6.
Lave', J., Avouac, J.P., 2001. Fluvial incision and tectonic uplift across the Himalayas of central Nepal. J. Geophys. Res. 106 (B11), 26561–26591. http://dx.doi.org/10.1029/2001JB000359.
Lemonnier, C., Marquis, G., Perrier, F., Avouac, J.-P., Chitrakar, G., Kafle, B., Sapkota, S., Gautam, U., Tiwari, D., Bano, M., 1999. Electrical structure of the Himalaya of central Nepal: high conductivity around the mid-crustal ramp along the MHT. Geophys. Res. Lett. 26 (21), 3261–3264. http://dx.doi.org/10.1029/1999GL008363.
Mahesh, P., Rai, S.S., Sivaram, K., Paul, A., Gupta, Sandeep, Sarma, Rajagopala, Gaur, V.K., 2013. One dimensional reference velocity model and precise locations of earthquake hypocenters in the Kumaon–Garhwal Himalaya. Bull. Seismol. Soc. Am. 103 (1), 328–339.
Michael, A.J., 1984. Determination of stress from slip data: faults and folds. J. Geophys. Res. 89, 11,517–11,526.
Michael, A.J., 1987. Use of focal mechanisms to determine stress: a control study. J. Geophys. Res. 92, 357–368.
Molnar, P., 1990. A review of the seismicity and the rates of active thrusting and deformation at the Himalaya. J. Himal. Geol. 1, 131–154.
Molnar, P., Chen, W.P., 1982. Seismicity and mountain building. In: Hsu, K.J. (Ed.), Mountain Building Processes. Academic, New York, pp. 41–57.
Mugnier, J.L., Huyghe, P., Leturmy, P., Jouanne, F., 2003. Episodicity and rates of thrust sheet motion in Himalayas (Western Nepal). Thrust Tectonics and Hydrocarbon Systems, McClay, AAPG Mem.
Murphy, M.A., Saylor, J.E., Ding, L., 2009. Late Miocene topographic inversion in Southwest Tibet based on integrated paleoelevation reconstructions and structural history. Earth Planet. Sci. Lett. 282, 1–9. http://dx.doi.org/10.1016/j.epsl.2009.01.006.
Nelson, K., 1996. Partially molten middle crust beneath southern Tibet: synthesis of project INDEPTH results. Science 274, 1684–1688.
Ni, J., Barazangi, M., 1984. Seismotectonics of the Himalayan collision zone: geometry of the underthrusting Indian plate beneath the Himalaya. J. Geophys. Res. 89, 1147–1163.
Pandey, M.R., Tandukar, R.P., Avouac, J.P., Lave, J., Massot, J.P., 1995. Interseismic strain accumulation on the Himalayan crustal ramp (Nepal). Geophys. Res. Lett. 22 (7), 751–754. http://dx.doi.org/10.1029/94GL02971.
Patel, R.C., Carter, A., 2009. Exhumation history of the higher Himalayan crystalline along Dhauliganga–Goriganga river valleys, NW India: new constraints from fission-track analysis. Tectonics 28. http://dx.doi.org/10.1029/2008TC002373.
Patel, R.C., Vikas, A., Singh, P., Kumar, Y., Lal, N., 2011a. Geology, structural and exhumation history of the higher Himalayan crystallines in Kumaon Himalaya, India. J. Geol. Soc. India 77 (1), 47–72.
Patel, R.C., Adlakha, V., Lal, N., Singh, P., Kumar, Y., 2011b. Spatiotemporal variation in exhumation of the crystallines in the NW-Himalaya, India: constraints from fission track dating analysis. Tectonophysics 504 (1–4), 1–13. http://dx.doi.org/10.1016/j.tecto.2010.11.011.
Patriat, P., Achache, J., 1984. India–Asia collision chronology has implications for crustal shortening and driving mechanism of plates. Nature 311, 615–621.
Paul, S.K., 1985. Structural and Petrological Studies of Munsiari–Dharchula area, Great Himalaya in Kumaun (Unpubl. Ph. D. Thesis). Kumaun University, Nainital, p. 135.
Paul, A., Bhakuni, S.S., Pant, C.C., Darmwal, G.S., Pathak, V., 2010. Microseismicity in central part of Inner Kumaun Lesser Himalaya: implication to active seismotectonics. Himal. Geol. 31 (2), 107–115.
Rajendran, C.P., Rajendran, K., 2005. The status of central seismic gap: a perspective based on the spatial and temporal aspect of the large Himalayan earthquakes. Tectonophysics 395, 19–39.
Robert, X., van der Beek, P., Braun, J., Perry, C., Mugnier, J.-L., 2011. Control of detachment geometry on lateral variations in exhumation rates in the Himalaya: insights from low-temperature thermochronology and numerical modeling. J. Geophys. Res. 116 (B5), B05202. http://dx.doi.org/10.1029/2010JB007893.
Schulte-Pelkum, V., Monsalve, G., Sheehan, A., Pandey, M.R., Sapkota, S., Bilham, R., Wu, F., 2005. Imaging the Indian subcontinent beneath the Himalaya. Nature 435, 1222–1225.
Searle, M.P., Law, R., Godin, L., Larson, K.P., Streule, M.J., Cottle, J., Jessup, M.J., 2008. Defining the Himalayan Main Central Thrust in Nepal. J. Geol. Soc. Lond. 165, 523–534.
Seeber, L., Armbuster, J.G., 1981. Great detachment earthquakes along the Himalayan arc and long-term forecasts. In: Simpson, D.W., Richards, P.G. (Eds.), Earthquake Prediction, An International Review, Maurice Ewing Series 4. Am. Geophys. Union, Washington, DC, pp. 259–279.
Singh, P., Patel, R.C., Lal, N., 2012. Plio-Plistocene in-sequence thrust propagation along the Main Central Thrust zone (Kumaon–Garhwal Himalaya, India): new thermochronological data. Tectonophysics 574–575, 193–203. http://dx.doi.org/10.1016/j.tecto.2012.08.015.
Srivastava, P., Mitra, G., 1994. Thrust geometries and deep structure of the outer and lesser Himalaya, Kumaun and Garhwal (India): implication for evolution of the Himalaya fold-and-thrust belt. Tectonics 13 (1), 89–109. http://dx.doi.org/10.1029/93TC01130.
Thakur, V.C., 1993. Geology of Western Himalaya. Pergamon Press (366p.).
Thakur, V.C., 2004. Active tectonics of Himalayan frontal thrust and seismic hazard to Ganga Plain. Curr. Sci. 86, 1554–1560.

Valdiya, K.S., 1976. Himalayan transverse faults and folds and their parallelism with subsurface structures of North Indian Plains. Tectonophysics 32, 353–386.
Valdiya, K.S., 1980. Geology of the Kumaon Lesser Himalaya. Wadia Institute of Himalaya, Dehra Dun, India (291 pp.).
Wobus, C.W., Whipple, K.X., Hodges, K.V., 2006. Neotectonics of the central Nepalese Himalaya: constraints from geomorphology, detrital $^{40}Ar/^{39}Ar$ thermochronology, and thermal modeling. Tectonics 25 (4), TC4011. http://dx.doi.org/10.1029/2005TC001935.
Yin, A., 2006. Cenozoic tectonic evolution of the Himalayan orogen as constrain by along strike variation of structural geometry, exhumation history and foreland sedimentation. Earth Sci. Rev. 76, 1–132.
Zhao, W., Nelson, K.D., Project INDEPTH Team, 1993. Deep seismic reflection evidence for continental underthrusting beneath southern Tibet. Nature 366, 557–559.